ChemComm

COMMUNICATION

View Article Online
View Journal | View Issue

Cite this: *Chem. Commun.*, 2025, **61**, 16989

Received 26th June 2025,
Accepted 23rd September 2025

DOI: 10.1039/d5cc03612g

rsc.li/chemcomm

Detection of SO_2 using a hybrid LDH-MOF material

Juan Andrés Flores-Aguilar,[ab] Marco L. Martínez,[ab] José Ortiz-Landeros,[c] Ariel Guzmán-Vargas,[a] Lazaro Huerta-Arcos,[d] Jose Antonio de los Reyes,[e] Valeria B. López-Cervantes,[b] Antonio Hernández-Monsalvo,[b] Diego Solis-Ibarra,[b] Andres de Luna Bugallo,*[f] Ilich A. Ibarra *[b] and Enrique Lima *[b]

A hybrid MgAlFe-LDH/UiO-66-NH_2 material has been developed for the efficient detection of SO_2, showing an exceptionally low detection limit of only 0.72 ppm, which is considerably lower in comparison to UiO-66-NH_2 (739 ppm). Spectroscopic studies suggest that the preferential oxidation of SO_2 to SO_4^{2-}, catalysed by the Fe^{3+} centres within MgAlFe-LDH, is the key factor in the enhanced fluorescence response. This process *in situ* generates Fe^{2+} sites and favours the interlaminar sequestration of SO_2, preventing direct interaction with the active sites of UiO-66-NH_2.

Sulphur dioxide (SO_2) is a colourless, pungent-smelling, highly irritating gas that is found in a gaseous state under standard ambient conditions (25 °C and 1 atmosphere). It is classified as a primary pollutant and its presence in the atmosphere is due to direct emissions from natural sources and human activities.[1]

Natural sources of emissions include volcanoes, which release significant volumes of this gas during their eruptions, together with the oxidation of organic materials in vegetation fires and agricultural practices involving biomass burning.[2] However, in the current context, industrial activity is the main source of emissions, particularly the combustion of sulphur rich energy resources such as certain types of coal and heavy oil fractions.[3] Even at low concentrations, uncontrolled SO_2 emissions pose risks to the environment and human health.[4] Their role in forming acid rain, which damages ecosystems, is exacerbated by their correlation with respiratory and cardiovascular diseases in exposed populations.[5] This duality of effects has prompted the need for highly accurate and sensitive monitoring systems. Therefore, measurement strategies that can accurately identify SO_2 at minimum thresholds ($\geq$1.5 ppm) in both dry and humid environments are required.[6]

Currently, resistive chemical sensors based on metal oxide semiconductors (such as SnO_2, WO_3 and TiO_2) are gaining prominence, due to their high sensitivity and selectivity towards SO_2, as well as their fast response and recovery kinetics.[7–11] However, their main limitation is their high operating temperature of 200–600 °C, which results in high energy consumption and limits their practical applications.[12–15] Therefore, developing materials that can detect SO_2 at room temperature and at low concentrations has become a priority. This breakthrough would mitigate problems associated with energy consumption and mark a fundamental milestone in the design of next-generation materials.

In this context, various porous materials have been investigated, among which lamellar double hydroxides (LDHs) and metal–organic frameworks (MOFs) stand out due to their potential for SO_2 adsorption and detection. LDHs correspond to lamellar ionic compounds with a brucite-like structure, where positively charged layers alternate with interlaminar regions containing compensating anions and water molecules.[16–18] Due to their unique structural properties, LDHs have attracted great attention for sensor and SO_2 capture applications.[19–21] However, they have certain disadvantages, such as limited selectivity and lower efficiency compared to other more developed materials.[22]

On the other hand, MOFs represent a class of highly crystalline porous materials, constituted by the coordinated bonding between metal centres and organic ligands, predominantly carboxylates.[23] These structures are distinguished by their high surface area, the possibility to modulate the pore size and the ability to adjust their physicochemical properties.[24–27] Thanks to these characteristics, MOFs are emerging as promising

[a] *Laboratorio de Investigación en Materiales Porosos, Catálisis Ambiental y Química Fina, Instituto Politécnico Nacional, ESIQIE-SEPI-DIQI, UPALM Edif. 7 P.B. Zacatenco, GAM, 07738 CDMX, Mexico*
[b] *Laboratorio de Fisicoquímica y Reactividad de Superficies (LaFReS), Instituto de Investigaciones en Materiales, Universidad Nacional Autónoma de México, Circuito Exterior s/n, CU, Coyoacán, 04510, Ciudad de Mexico, Mexico. E-mail: argel@unam.mx, lima@iim.unam.mx*
[c] *Departamento de Ingeniería en Metalurgia y Materiales, Instituto Politécnico Nacional-ESIQIE, Zacatenco, Ciudad de Mexico 07738, Mexico*
[d] *Investigaciones en Materiales, Universidad Nacional Autónoma de Mexico, Circuito Exterior s/n, CU, Coyoacán, 04510, Ciudad de Mexico, Mexico*
[e] *Departamento de Ingeniería de Procesos e Hidráulica, División de Ciencias Basicas e Ingeniería, Universidad Autónoma Metropolitana-Iztapalapa, 09340, Ciudad de Mexico, Mexico*
[f] *Centro de Física Aplicada y Tecnología Avanzada, Campus UNAM, 76230, Juriquilla, Querétaro, Mexico. E-mail: aluna@fata.unam.mx*

candidates for use in detecting and capturing toxic and corrosive gases such as SO_2. Recently, MOFs have emerged as promising materials in the field of luminescence due to their structure. These characteristics allow them to modulate their fluorescence, providing a flexible possibility to design materials with specific optical responses.[28] Luminescence in MOFs can be originated through different mechanisms, which postulates them as ideal candidates for the selective detection of analytes.[29] However, most MOFs exhibit marked instability upon exposure to moisture and acid gases (*e.g.*, SO_2). Thus, the development of hybrid MOF-LDH-type materials with unique properties that can improve both the specific interaction with SO_2 and their detection through specific fluorescence-mediated changes has been studied, opening new possibilities for the development of efficient sensors.

With this target in mind, an effective MOF-LDH hybrid material was successfully developed. The MgAlFe-LDH/UiO-66-NH_2 composite was synthesised through the surface functionalisation of MgAlFe-LDH using the coupling agent CPTMS (3-chloropropyltrimethoxysilane), which acted as a molecular bridge for the covalent anchoring of UiO-66-NH_2 *via in situ* growth. The methoxy (–OCH_3) groups of the CPTMS reacted with the hydroxyl (–OH) groups on the surface of MgAlFe-LDH, while the chlorinated end (–CH_2Cl) of the silane generated an electrophilic centre after chlorine removal, capable of reacting with the carboxyl (–COOH) groups from the UiO-66-NH_2 ligand (Fig. S1, SI). This covalent coupling mechanism enabled a stable interface to be formed between the two materials.

Powder X-ray diffraction (PXRD), FT-IR spectroscopy, scanning electron microscopy (SEM) and thermogravimetric analysis (TGA) were used to confirm the phase purity of MgAlFe-LDH, MgAlFe-LDH-CPTMS, UiO-66-NH_2 and MgAlFe-LDH/UiO-66-NH_2 (Fig. S2–S6, SI). Additionally, XPS analysis was performed to confirm the effective functionalisation of the materials. High-resolution XPS analysis of the O 1s region (Fig. S7a, SI) confirms the surface modification of MgAlFe-LDH with CPTMS, as indicated by the appearance of a new peak at 533.1 eV (Si–O) and a shift of the O–M peak (M═Mg, Al, Fe) towards higher energies, indicative of the formation of covalent bonds between MgAlFe-LDH and the organosilane. In the case of MgAlFe-LDH/UiO-66-NH_2 (Fig. S7b, SI), the shift of the O–M peak (530.5 eV) confirms the presence of the O–M bonds (O–Al, O–Mg and O–Zr) of both MgAlFe-LDH and UiO-66-NH_2. The changes in the signals at 532.0 eV (decrease in area) and 532.9 eV (an increase in area) reflect covalent interactions between the carboxyl groups of the UiO-66-NH_2 ligand and CPTMS, as well as the formation of new Si–O bonds during the *in situ* growth of UiO-66-NH_2 on the modified MgAlFe-LDH. These results validate the successful functionalisation of the hybrid system through covalent bonds.

The surface area and pore diameter of the different sintered materials were subsequently evaluated using N_2 physisorption at −196 °C (77 K) (Fig. S8 and Table S1, SI). SO_2 adsorption–desorption isotherms were carried out using a DVS vacuum (Surface Measurement Systems Ltd) dynamic gravimetric gas/vapour sorption analyser from 0 to 0.1 bar at 25 °C for the activated samples MgAlFe-LDH, UiO-66-NH_2 and MgAlFe-LDH/UiO-66-NH_2. Fig. 1 shows the resulting isotherms. Typical type I behaviour was observed, with pronounced SO_2 sorption in the 0.03 bar range. Values reached 1.4 mmol g^{-1} for UiO-66-NH_2, 1.2 mmol g^{-1} for MgAlFe-LDH/UiO-66-NH_2, and 0.49 mmol g^{-1} for MgAlFe-LDH. As the pressure increased from 0.03 to 0.1 bar, the adsorption capacity increased gradually to 2.1 mmol g^{-1} (UiO-66-NH_2), 1.78 mmol g^{-1} (MgAlFe-LDH/UiO-66-NH_2) and 0.59 mmol g^{-1} (MgAlFe-LDH), respectively.

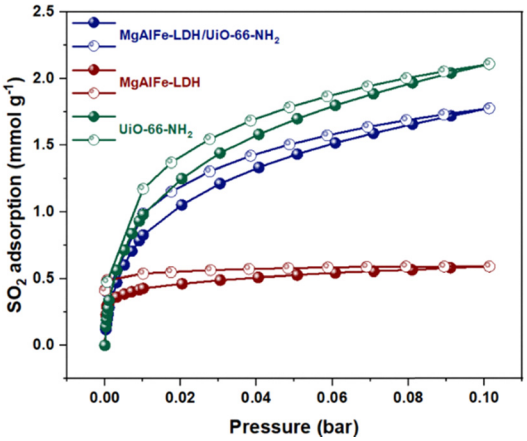

Fig. 1 The SO_2 isotherms of MgAlFe-LDH/UiO-66-NH_2, MgAlFe-LDH and UiO-66-NH_2 at 25 °C and 0.1 bar. Filled circles = adsorption; hollow circles = desorption.

The results indicate that UiO-66-NH_2 exhibits a higher SO_2 adsorption capacity than MgAlFe-LDH/UiO-66-NH_2 and MgAlFe-LDH. This difference between UiO-66-NH_2 and MgAlFe-LDH/UiO-66-NH_2 was mainly attributed to structural modifications induced during the functionalisation process. In MgAlFe-LDH/UiO-66-NH_2, the incorporation of MgAlFe-LDH could alter the crystalline orientation of the MOF, generating a partial blockage of its porosity and reducing accessibility to the active sites. In contrast, UiO-66-NH_2 retains its porous integrity and homogeneous crystalline arrangement, favouring more efficient interactions with SO_2 molecules. These observations are consistent with BET surface area analyses, which indicates a substantial decrease in the specific surface area of MgAlFe-LDH/UiO-66-NH_2 relative to UiO-66-NH_2. By contrast, the results for MgAlFe-LDH were consistent with those reported in the literature.[30] The most significant property of a material for SO_2 detection is probably its adsorption capacity under low pressures ($P < 0.1$ bar), since the typical concentration ranges for SO_2 detection (generally measured in ppm) have a direct correlation with the low-pressure regime of the gas.[31] In this context, the SO_2 adsorption behaviour of MgAlFe-LDH, UiO-66-NH_2 and MgAlFe-LDH/UiO-66-NH_2 was evaluated and the possibility of using these materials as SO_2 detectors was investigated. Specifically, it was expected that the MgAlFe-LDH/UiO-66-NH_2 hybrid material would demonstrate superior fluorescent properties for SO_2 detection.

First, the UV-Vis spectra of UiO-66-NH_2 and MgAlFe-LDH/UiO-66-NH_2 (Fig. S9, SI) reveal bands that are characteristic of electronic transitions within different spectral ranges. Between 250 and 300 nm, bands are observed that are attributable to $\pi \rightarrow \pi^*$ transitions, while in the 300–400 nm region, the bands

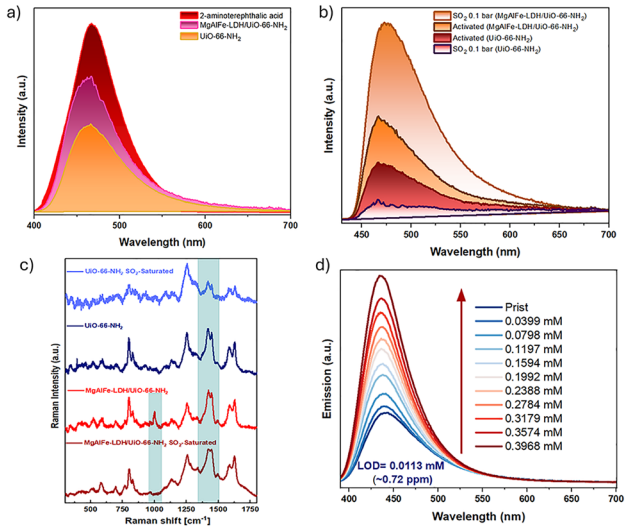

Fig. 2 (a) Comparison of the emission spectra of the 2-aminoterephthalic acid linker, UiO-66-NH_2 and MgAlFe-LDH/UiO-66-NH_2. (b) Comparison of the emission spectra of activated UiO-66-NH_2 and MgAlFe-LDH/UiO-66-NH_2 samples, exposed to 0.1 bar SO_2. (c) Comparison of the RAMAN spectra of activated UiO-66-NH_2 and MgAlFe-LDH/UiO-66-NH_2 samples, exposed to 0.1 bar SO_2. (d) Emission spectra of MgAlFe-LDH/UiO-66-NH_2 suspensions in THF exposed to SO_2.

correspond to n → π* transitions.[32–34] Conversely, MgAlFe-LDH shows an absorption band below 300 nm attributable to π transitions from OH^- orbitals to Fe^{3+} 3d orbitals, and between 300 and 500 nm, absorption bands are observed that could be related to iron clusters.[35]

In order to evaluate the emission properties and determine the optimum excitation wavelength, solid-state emission spectra were obtained for both UiO-66-NH_2 and MgAlFe-LDH/UiO-66-NH_2. For both materials, the best emission was found to be obtained at 380 nm, so this excitation wavelength was chosen for all fluorescence experiments. The emission spectra of the 2-aminoterephthalic acid ligand and the UiO-66-NH_2 and MgAlFe-LDH/UiO-66-NH_2 materials reveal marked differences in fluorescent behaviour (Fig. 2a). While the free ligand exhibits a characteristic emission at 467 nm associated with n–π* transitions,[36,37] the formation of UiO-66-NH_2 through coordination with Zr^{4+} results in significant fluorescent quenching due to ligand-metal charge transfer (LMCT). This phenomenon occurs when the excited electrons of the ligand are transferred to the empty orbitals of Zr^{4+}, preventing radiative recombination and consequently suppressing the emission.[38–41] Interestingly, MgAlFe-LDH/UiO-66-NH_2 exhibits increased emission intensity compared to UiO-66-NH_2, possibly due to the presence of Fe^{3+} in the MgAlFe-LDH structure. This inhibits the LMCT process characteristic of UiO-66-NH_2 by acting as a less favourable electron-accepting centre than Zr^{4+}. This reduces the non-radiative deactivation pathways. This behaviour is consistent with that observed in the UV-Vis spectra (Fig. S9, SI), where the band associated with the n → π transitions (the LMCT-associated band) in MgAlFe-LDH/UiO-66-NH_2 is found to decrease in intensity relative to UiO-66-NH_2.

Once the fluorescence behaviour of UiO-66-NH_2 and MgAlFe-LDH/UiO-66-NH_2 was observed, solid-state SO_2 detection was evaluated, where activated samples (120 °C for 3 hours) of UiO-66-NH_2 and MgAlFe-LDH/UiO-66-NH_2 were exposed to 0.1 bar SO_2 to observe what changes occur in their photoluminescence properties. Interestingly, opposite behaviours were observed between the materials: UiO-66-NH_2 exhibited a fluorescent quenching of 42.5% (Fig. 2b), attributed to the polarisation of the lone pairs (n) of the $-NH_2$ group by the SO_2 dipole moment. RAMAN spectra confirm this interaction (Fig. 2c), showing a decrease in the characteristic bands of the $-NH_2$ group (1300–1500 cm^{-1}); conversely the MgAlFe-LDH/UiO-66-NH_2 hybrid compound exhibited a 191.45% increase in the fluorescence emission intensity, which was attributed to the catalytic oxidation of SO_2 to SO_4^{2-}, mediated by the Fe^{3+} centres of the MgAlFe-LDH.[30] This was confirmed by the disappearance of the CO_3^{2-} band (~1060 cm^{-1}) in the Raman spectra (Fig. 2c and Fig. S10, SI) and the appearance of the asymmetric S–O stretch (~1100 cm^{-1}) in the FTIR spectra (Fig. S11, SI). This process restricts SO_2 diffusion to the active sites of UiO-66-NH_2, while *in situ* Fe^{2+} generation (Fig. S12, SI) acts as an electron donor to the ligand's π-conjugated system. This demonstrates that the synergy between the hybrid material's components allows its fluorescent response to be modulated by a redox mechanism and the physical blocking effect of SO_2.

Finally, the limit of detection (LOD) of MgAlFe-LDH/UiO-66-NH_2 was experimentally determined in a suspension of the material in THF, obtaining a value of 0.72 ppm (Fig. 2d), demonstrating its high potential as an efficient SO_2 sensor. This result represents a huge improvement compared to the LOD of UiO-66-NH_2 (739 ppm) (Fig. S20, SI), showing that the synergistic interaction between MgAlFe-LDH and UiO-66-NH_2 significantly enhances the sensitivity of the material.

To summarise, the MgAlFe-LDH/UiO-66-NH_2 hybrid material was demonstrated to be capable of adsorbing SO_2 under low pressures (1.2 mmol g^{-1} at 0.03 bar) with an excellent fluorescence sensitivity response. In contrast to UiO-66-NH_2, which exhibited turn-off behaviour in fluorescence, the hybrid compound demonstrated a turn-on effect in fluorescence emission, achieving an exceptional SO_2 detection limit of 0.72 ppm. Spectroscopic studies revealed that this behaviour is due to the catalytic oxidation of SO_2 being mediated by the Fe^{3+} centres of MgAlFe-LDH, as well as the capture of SO_2 in the interlaminar part of MgAlFe-LDH, which modulates the interaction with UiO-66-NH_2. Overall, this study demonstrates that the strategic combination of the properties of LDHs and MOFs can overcome the limitations of individual materials, providing a fundamental design principle for the development of hybrid materials, in which optimising the ratio and arrangement of the components will enable superior sensitivity and selectivity to be achieved in gas detection.

J. A. F. A. and M. L. M. thank SECIHT for the PhD fellowships (1176665 and 1080048). J. A. F. A. thanks V. M. S. P. for her valuable scientific inspiration and assistance with artistic consultation. E. L. thanks Secihti (CBF 2023-2024-227) and I. A. I. thanks PAPIIT UNAM (IN201123), México, for financial support.

We thank U. Winnberg (Euro Health) for scientific discussions and G. Ibarra-Winnberg for scientific encouragement.

Conflicts of interest

There are no conflicts to declare.

Data availability

The datasets supporting this article are provided in the supplementary information (SI). Supplementary information: synthesis, characterization, and additional figures and tables. See DOI: https://doi.org/10.1039/d5cc03612g.

References

1 P. Amoatey, H. Omidvarborna, M. S. Baawain and A. Al-Mamun, *Process Saf. Environ. Prot.*, 2019, **123**, 215–228.
2 S. A. Carn, V. E. Fioletov, C. A. Mclinden, C. Li and N. A. Krotkov, *Sci. Rep.*, 2017, **7**, 44095.
3 F. Liu, S. Choi, C. Li, V. E. Fioletov, C. A. McLinden, J. Joiner, N. A. Krotkov, H. Bian, G. Janssens-Maenhout, A. S. Darmenov and A. M. Da Silva, *Atmos. Chem. Phys.*, 2018, **18**, 16571–16586.
4 E. Martínez-Ahumada, D. He, V. Berryman, A. López-Olvera, M. Hernandez, V. Jancik, V. Martis, M. A. Vera, E. Lima, D. J. Parker, A. I. Cooper, I. A. Ibarra and M. Liu, *Angew. Chem., Int. Ed.*, 2021, **60**, 17556–17563.
5 E. Martínez-Ahumada, M. L. Díaz-Ramírez, H. A. Lara-García, D. R. Williams, V. Martis, V. Jancik, V. Jancik, E. Lima and I. A. Ibarra, *J. Mater. Chem. A*, 2020, **8**, 11515–11520.
6 S. D. J. Valencia-Loza, A. López-Olvera, E. Martínez-Ahumada, D. Martínez-Otero, I. A. Ibarra, V. Jancik and E. G. Percástegui, *ACS Appl. Mater. Interfaces*, 2021, **13**, 18658–18665.
7 F. Berger, M. Fromm, A. Chambaudet and R. Planade, *Sens. Actuators, B*, 1997, **45**, 175–181.
8 H. Torvela, J. Huusko and V. Lantto, *Sens. Actuators, B*, 1991, **4**, 479–484.
9 Y. Shimizu, N. Matsunaga, T. Hyodo and M. Egashira, *Sens. Actuators, B*, 2001, **77**, 35–40.
10 M. Stankova, X. Vilanova, J. Calderer, E. Llobet, P. Ivanov, I. Grácia, C. Cané and X. Correig, *Sens. Actuators, B*, 2004, **102**, 219–225.
11 M. Penza, G. Cassano and F. Tortorella, *Sens. Actuators, B*, 2001, **81**, 115–121.
12 M. Gardon and J. M. Guilemany, *J. Mater. Sci.:Mater. Electron.*, 2013, **24**, 1410–1421.
13 N. Barsan, D. Koziej and U. Weimar, *Sens. Actuators, B*, 2007, **121**, 18–35.
14 D. E. Williams, *Sens. Actuators, B*, 1999, **57**, 1–16.
15 T. Hübert, L. Boon-Brett, G. Black and U. Banach, *Sens. Actuators, B*, 2011, **157**, 329–352.
16 Q. Wang and D. Ohare, *Chem. Rev.*, 2012, **112**, 4124–4155.
17 C. Forano, U. Costantino, V. Prévot and C. T. Gueho, *Developments in Clay Science*, Elsevier B.V., 2013, vol. 5, pp. 745–782.
18 D. Chaillot, S. Bennici and J. Brendlé, *Environ. Sci. Pollut. Res.*, 2021, **28**, 24375–24405.
19 T. Kameda, Y. Takahashi, S. Kumagai, Y. Saito, S. Fujita, I. Itou, T. Han and T. Yoshioka, *Inorg. Chem. Commun.*, 2022, **135**, 109108.
20 T. Kameda, Y. Takahashi, S. Kumagai, Y. Saito, S. Fujita, I. Itou, T. Han and T. Yoshioka, *J. Porous Mater.*, 2022, **29**, 723–728.
21 R. B. Shinde, N. S. Padalkar, S. V. Sadavar, S. B. Kale, V. V. Magdum, Y. M. Chitare, S. P. Kulkarni, U. M. Patil, V. G. Parale, H. H. Park and J. L. Gunjakar, *J. Hazard. Mater.*, 2022, **432**, 128734.
22 Y. Zhang, L. Zhao, M. Kang, Z. Chen, S. Gao and H. Hao, *Chem. Eng. J.*, 2021, **426**, 131873.
23 H. C. Zhou, J. R. Long and O. M. Yaghi, *Chem. Rev.*, 2012, **112**, 673–674.
24 Z. Bao, J. Wang, Z. Zhang, H. Xing, Q. Yang, Y. Yang, H. Wu, R. Krishna, W. Zhou, B. Chen and Q. Ren, *Angew. Chem.*, 2018, **130**, 16252–16257.
25 L. Li, L. Guo, Z. Zhang, Q. Yang, Y. Yang, Z. Bao, Q. Ren and J. Li, *J. Am. Chem. Soc.*, 2019, **141**, 9358–9364.
26 Y. Gurdal and S. Keskin, *Ind. Eng. Chem. Res.*, 2012, **51**, 7373–7382.
27 V. B. López-Cervantes, J. L. Obeso, A. Yañez-Aulestia, A. Islas-Jácome, C. Leyva, E. González-Zamora, E. Sánchez-González and I. A. Ibarra, *Chem. Commun.*, 2023, **59**, 10343–10359.
28 V. B. López-Cervantes, M. L. Martínez, J. L. Obeso, C. García-Carvajal, N. S. Portillo-Vélez, A. Guzmán-Vargas, R. A. Peralta, E. González-Zamora, I. A. Ibarra, D. Solis-Ibarra, J. L. Woodliffe and Y. A. Amador-Sánchez, *Dalton Trans.*, 2025, **54**, 1646–1654.
29 P. Brandt, A. Nuhnen, M. Lange, J. Möllmer, O. Weingart and C. Janiak, *ACS Appl. Mater. Interfaces*, 2019, **11**, 17350–17358.
30 H. T. Kang, K. Lv and S. L. Yuan, *Appl. Clay Sci.*, 2013, **72**, 184–190.
31 P. Brandt, S. H. Xing, J. Liang, G. Kurt, A. Nuhnen, O. Weingart and C. Janiak, *ACS Appl. Mater. Interfaces*, 2021, **13**, 29137–29149.
32 T. T. Cai, Y. Tian, P. Huang and F. Y. Wu, *Anal. Chim. Acta*, 2022, **1235**, 340550.
33 H. Assi, L. C. Pardo Pérez, G. Mouchaham, F. Ragon, M. Nasalevich, N. Guillou, C. Martineau, H. Chevreau, F. Kapteijn, J. Gascon, P. Fertey, E. Elkaim, C. Serre and T. Devic, *Inorg. Chem.*, 2016, **55**, 7192–7199.
34 W. Zhang, L. Wang and J. Zhang, *Res. Chem. Intermed.*, 2019, **45**, 4801–4811.
35 A. Seijas-Da Silva, V. Oestreicher, E. Coronado and G. Abellán, *Dalton Trans.*, 2022, **51**, 4675–4684.
36 Y. Q. Sun, Y. Cheng and X. B. Yin, *Anal. Chem.*, 2021, **93**, 3559–3566.
37 W. Bai, G. Qin, J. Wang, L. Li and Y. Ni, *Dyes Pigm.*, 2021, **193**, 109473.
38 K. F. Kayani and A. M. Abdullah, *J. Food Compos. Anal.*, 2024, **135**, 106577.
39 L. Xia, W. Zhou, Y. Xu, Z. Xia, X. Wang, Q. Yang, G. Xie, S. Chen and S. Gao, *Chem. Eng. J.*, 2023, **451**, 138747.
40 S. Q. Wang, X. Gu, X. Wang, X. Y. Zhang, X. Y. Dao, X. M. Cheng, J. Ma and W. Y. Sun, *Chem. Eng. J.*, 2022, **429**, 132157.
41 J. A. Flores-Aguilar, M. L. Martínez, V. B. López-Cervantes, A. Guzmán-Vargas, J. Ortiz-Landeros, A. de, L. Bugallo, D. Solis-Ibarra, I. A. Ibarra and E. Lima, *ACS Appl. Opt. Mater.*, 2025, **3**(9), 2013–2025.

